Emergent phases and critical behavior in a non-Markovian open quantum system

H. F. H. Cheung, Y. S. Patil, and M. Vengalattore

Emergent phases and novel critical behavior in a non-Markovian open quantum system

H. F. H. Cheung, Y. S. Patil and M. Vengalattore

Laboratory of Atomic and Solid State Physics, Cornell University, Ithaca, NY 14853[*]

Open quantum systems exhibit a range of novel out-of-equilibrium behavior due to the interplay between coherent quantum dynamics and dissipation. Of particular interest in these systems are driven, dissipative transitions, the emergence of dynamical phases with novel broken symmetries, and critical behavior that lies beyond the conventional paradigm of Landau-Ginzburg phenomenology. Here, we consider a parametrically driven two-mode system in the presence of non-Markovian system-reservoir interactions. We show that the non-Markovian dynamics modifies the phase diagram of this system resulting in the emergence of a novel broken symmetry phase in a new universality class that has no counterpart in the corresponding Markovian system. This emergent phase is accompanied by enhanced two-mode entanglement that remains robust at finite temperatures. Such reservoir-engineered dynamical phases can potentially shed light on universal aspects of dynamical phase transitions in a wide range of non-equilibrium systems, and aid in the development of techniques for the robust generation of entanglement and quantum correlations at finite temperatures with potential applications to quantum control, state preparation and metrology.

I. INTRODUCTION

Due to the commensurate influence of quantum coherence and dissipation, the dynamical behavior of open quantum systems conforms neither to the framework of unitary quantum evolution nor to thermodynamic descriptions [1, 2]. Motivated by various applications to quantum information science, experimental realizations of such open systems have been developed in platforms spanning trapped ions [3], circuit-QED systems [4], optomechanical systems [5] and hybrid quantum systems [6]. The exploration of novel dynamical phases and the development of techniques for robust quantum state preparation and control in these systems presents significant theoretical and experimental challenges that lie at the interface of atomic physics, quantum optics, and condensed matter physics.

In addition to the traditional approach of Hamiltonian design, open quantum systems are amenable to control by modifying the nature of their environment. As such, the concept of reservoir-engineering [7] has emerged as a promising paradigm for the realization of novel states of open and driven quantum systems. In certain cases, it has been shown that reservoir-engineering can be used to coax the open quantum system into phases that might not be accessible through more conventional forms of quantum state preparation [8, 9]. Aside from presenting alternate routes to quantum state preparation, such reservoir-engineered quantum phases present intriguing questions in their own right. For instance, it is unclear to what extent driven, dissipative transitions in open quantum systems accommodate the central paradigms of scale invariance, symmetry breaking and universality that underpin our understanding of equilibrium and quantum phase transitions.

Here, we explore the driven, dissipative transitions of a parametrically driven two-mode quantum system in the presence of a non-Markovian environment. This is a minimal physical realization of the parametric oscillator model [10, 11] and is closely connected to the open Dicke model [12–14], the superradiant phase transition [15] and the Lipkin-Meshkov-Glick model [16]. In the presence of a Markovian reservoir, it has been shown that this system exhibits a non-equilibrium phase transition into an ordered state that develops beyond a critical magnitude of the external drive [17]. Further, recent work has shown that the presence of a sub-ohmic reservoir modifies the critical exponents of this non-equilibrium transition while preserving the steady-state phase diagram [18–20].

In this work, we go beyond these prior results and identify a class of experimentally accessible non-Markovianity that leads to significant changes in the phase diagram of this system, leading to the emergence of a dynamical phase with novel broken symmetries and critical behavior that is distinct from that observed in the Markovian system. We also demonstrate that this novel emergent phase manifests significantly enhanced correlations and entanglement than can be realized in the corresponding Markovian system. This two-mode entanglement is shown to persist even at finite temperatures and is a unique feature of the non-Markovian system-reservoir dynamics that allows for the backflow of information from the environment back into the system [21, 22]. This robust entan-

glement is distinct from Markovian system-reservoir dynamics that usually results in an irreversible loss of information and correlations into the environment. As such, our work points to an experimentally realizable instance where reservoir engineering techniques aid in the creation of robust, finite temperature correlations and entanglement with applications to various forms of metrology and quantum information processing.

II. MODEL

The Hamiltonian of our system is [23, 24]

$$\mathcal{H}/\hbar = \sum_k \omega_k \hat{a}_k^\dagger \hat{a}_k - \chi \hat{x}_P \hat{x}_i \hat{x}_s - (F_P e^{-i\omega_P t} \hat{a}_P^\dagger + \text{h.c.})$$

where the indices $k = \{i, s, P\}$ denote the idler, signal and pump modes at frequencies ω_k, and $\hat{a}_k$ denote their annihilation operators. The second term represents a two-mode interaction of strength χ between the signal and idler modes mediated by the actively driven pump. The third term represents the classical drive of the pump mode with magnitude F_P at its resonant frequency ω_P. The influence of the reservoir is incorporated through a master equation [25] and leads to Heisenberg-Langevin equations of the form

$$\dot{a}_i = -\frac{1}{2}\int_{-\infty}^t \gamma(t-t')a_i(t')dt' + iga_s^\dagger a_P + if_i$$

$$\dot{a}_s = -\frac{1}{2}\int_{-\infty}^t \gamma(t-t')a_s(t')dt' + iga_i^\dagger a_P + if_s$$

$$\dot{a}_P = -\frac{\gamma_P}{2}a_P + iga_i a_s + iF_P$$

where $\gamma(t)$ is the dissipation kernel in the rotating frame, and is related to the Langevin forces $f_{i,s}$ through the fluctuation-dissipation theorem, and the normalized coupling strength is $g = \chi x_{0,i} x_{0,s} x_{0,P}$ with $x_{0,\{i,s,P\}}$ denoting the zero point amplitudes of the respective modes. In the above, we have made the rotating wave approximation, assumed that $\omega_P = \omega_i + \omega_s$ and that the damping rate of the pump mode γ_P is much larger than those of the signal and idler modes, in close accordance with experimental realizations of this model [23]. The equations of motion are invariant under the transformation $(\hat{a}_i, \hat{a}_s) \to (\hat{a}_i e^{+i\phi}, \hat{a}_s e^{-i\phi})$ for $\phi \in [0, 2\pi)$. In addition, the presence of the classical drive at the pump frequency implies that the equations of motion are also invariant under the transformation $(\hat{a}_i, \hat{a}_s, \hat{a}_P) \to (\hat{a}_i^\dagger, \hat{a}_s^\dagger, -\hat{a}_P^\dagger)$. Thus, the physical system possesses both a $U(1)$ symmetry and a $\mathbb{Z}_2$ symmetry.
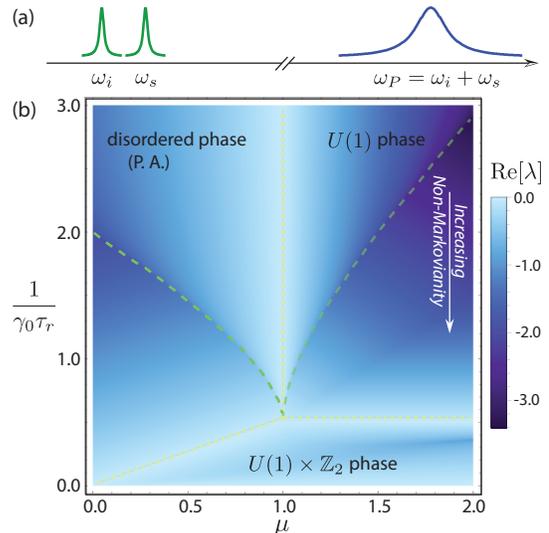
FIG. 1. (a) Schematic of the two-mode system. (b) The phase diagram as a function of the drive strength $\mu \equiv F_P/F_{cr}$ and the normalized reservoir decay rate $(\gamma_0 \tau_r)^{-1}$. The color scale indicates the least negative real part of the eigenvalues λ of the dynamical matrix (see text). Critical points and phase boundaries (white dashed lines) correspond to the vanishing of this real part, i.e. a divergent relaxation time. The non-Markovian system-reservoir dynamics leads to the formation of exceptional points both in the disordered phase and the $U(1)$ phase. The trajectory of these exceptional points is indicated by the green dashed lines. (see text).

For a Markovian reservoir, i.e. $\gamma(t) = \gamma_0 \delta(t)$, this system exhibits a continuous transition at a critical pump amplitude $F_{cr} = \frac{\gamma_P \gamma_0}{4g}$ from a disordered (parametric amplifier) phase to an ordered phase characterized by parametric self-oscillation of the signal and idler modes. This transition is accompanied by the spontaneous breaking of the $U(1)$ symmetry related to the difference between signal and idler phases [10, 24]. Similar phenomenology also arises in the closely related open Dicke model [12, 26].

Here, we consider the case where the signal and idler modes are in contact with a reservoir through a dissipation kernel $\gamma(t) = \gamma_0 \frac{e^{-t/\tau_r}}{\tau_r}$, where τ_r represents the coherence time or 'memory' of the non-Markovian reservoir. This form of non-Markovian dynamics arises naturally in the context of several cavity optomechanical systems [23, 24, 27, 28] as well as hybrid systems in which an optomechanical system is coupled to coherent ensembles of quantum spins [29, 30].

III. MEAN FIELD SOLUTIONS AND THE PHASE DIAGRAM

The Heisenberg-Langevin equations yield distinct steady state dynamical phases for this sytem. Such steady state solutions for the signal and idler modes can be represented by the form $a_{i,s} = |a_{i,s}|e^{i\theta_{i,s}}e^{-i\Delta_{i,s}t}$. The Heisenberg-Langevin equations can be linearized around these steady state solutions and cast in Fourier space as $-i\omega\mathbf{a} = \mathbf{\Sigma}\mathbf{a}+\mathbf{v}$ (see Appendix C). Here, $\mathbf{a} = (a_i, a_s, a_P)^T$, and the noise forces $\mathbf{v}$ are zero-mean gaussian variables whose correlation function is related to the dissipation kernel via the fluctuation-dissipation theorem. The eigenvalues λ of the inverse susceptibility matrix (or the dynamical matrix) $-\mathbf{\Sigma}-i\omega\mathbf{I}$ determine the low energy eigenspectrum and steady-state phase diagram of this system. Phase boundaries between dynamical states of distinct symmetries are associated with a vanishing of the least negative real part of the eigenvalues λ, i.e. a divergent relaxation time [31, 32]. The stability of the mean field dynamical phases to generic perturbations is indicated by non-positive real parts of the eigenvalues. The mean field solutions of this non-Markovian system allow for three stable dynamical phases (Fig. 1).

Disordered Phase : - In the limit of small pump drive, the intrinsic dissipation dominates the dynamics of the system. The steady state solution has a vanishing amplitude of the signal and idler modes. The nonlinear interaction between the two modes realizes a parametric amplifier with a phase-dependent gain that induces squeezing of composite quadratures formed from linear combinations of the signal and idler quadratures [24]. We denote this regime as the disordered or parametric amplifier (PA) phase.

U(1) Phase : - We first consider the regime of small reservoir coherence time, i.e. $(\gamma_0\tau_r)^{-1} \gg 1$. Note that the Markovian regime is obtained in the limit $(\gamma_0\tau_r)^{-1} \to \infty$. For a normalized pump drive $\mu = F_P/F_{cr} > 1$, the signal and idler modes exhibit parametric self-oscillation at their resonant frequencies $\omega_{i,s}$. The steady-state solutions are $\bar{a}_{i,s} = i\frac{\sqrt{\gamma_0\gamma_P}}{2g}e^{\pm i\phi/2}\sqrt{\mu-1}$. The $U(1)$ symmetry corresponding to the unconstrained phase difference ϕ between the signal and idler modes is spontaneously broken at the phase boundary $\mu_{cr} = 1$. As such, we denote this as the $U(1)$ phase. These solutions are consistent with the corresponding phases in a purely Markovian system.

U(1) × $\mathbb{Z}_2$ Phase : - In contrast, as the coherence time τ_r is increased, the system is qualitatively modified due to the competing effects of dissipation and reservoir coherence. As the timescales of these processes become

commensurate, the eigenvalues morph into complex conjugate pairs analogous to $\mathcal{PT}$ symmetry breaking. For $(\gamma_0\tau_r)^{-1} < \frac{1}{2}$, a new limit cycle phase emerges with the signal and idler modes either given by the solution $\bar{a}_i \propto ie^{i\phi/2}e^{-i\Delta t}\sqrt{\mu-\mu_{cr}}$, $\bar{a}_s \propto ie^{-i\phi/2}e^{i\Delta t}\sqrt{\mu-\mu_{cr}}$, or by the solution $\bar{a}_i \propto ie^{i\phi/2}e^{i\Delta t}\sqrt{\mu-\mu_{cr}}$, $\bar{a}_s \propto ie^{-i\phi/2}e^{-i\Delta t}\sqrt{\mu-\mu_{cr}}$. These solutions correspond respectively to a clockwise or counter-clockwise precession of the relative phase between these modes at an emergent limit cycle frequency $\Delta = \tau_r^{-1}\sqrt{\frac{\gamma_0\tau_r}{2}-1}$ that depends solely on the environmental parameters. The underlying $\mathbb{Z}_2$ symmetry reflecting these two choices is thus spontaneously broken in this limit cycle phase (see Fig. 2(a)). Further, the critical drive strength monotonically decreases as $\mu_{cr} = \frac{2}{\gamma_0\tau_r}$.

In this emergent limit cycle phase, the signal and idler modes exhibit self-oscillatory behavior not at their nominal resonances but at shifted frequencies $\omega_i \to \omega_i \pm \Delta, \omega_s \to \omega_s \mp \Delta$, with the choice of $\pm\Delta$ corresponding to a spontaneous breaking of a $\mathbb{Z}_2$ symmetry. In contrast to the fixed phase difference between the signal and idler modes in the $U(1)$ phase, the phases of these modes now oscillate at a rate Δ in this limit cycle phase. To further establish that this is a distinct phase, we calculate the dynamical states for a fixed drive $\mu > 1$ as the reservoir coherence time is reduced (Fig. 2(b)). We find that below the phase boundary $(\gamma_0\tau_r)^{-1} = \frac{1}{2}$, the limit cycle frequency Δ continuously grows from zero with its magnitude increasing as the square root of the distance from the critical point. We also compute the spectrum of Δ using a linearized equation, and find that its variance diverges at the $U(1) - U(1) \times \mathbb{Z}_2$ phase boundary, $(\gamma_0\tau_r)^{-1} = \frac{1}{2}$ (see Fig.2(b), Appendix F). The square root dependence of Δ below the critical point and the divergence of its noise spectrum are characteristic of a continuous phase transition with an order parameter Δ.

IV. EFFECT OF FLUCTUATIONS AND STABILITY OF THE MEAN FIELD PHASES

Here, we examine the stability of the mean field phases to generic gaussian perturbations. As described in the previous section, the stability of the mean field dynamical phases can be analyzed by evaluating the eigenspectrum of the dynamical matrix that governs the response of the various modes to perturbations. In particular, the stability of each of the dynamical phases is indicated by non-positive real parts of the eigenvalues λ of the dynamical matrix [31]. In other words, the mean field states are stable if the system responds to such perturbations by relaxing back to its steady state with a finite damping
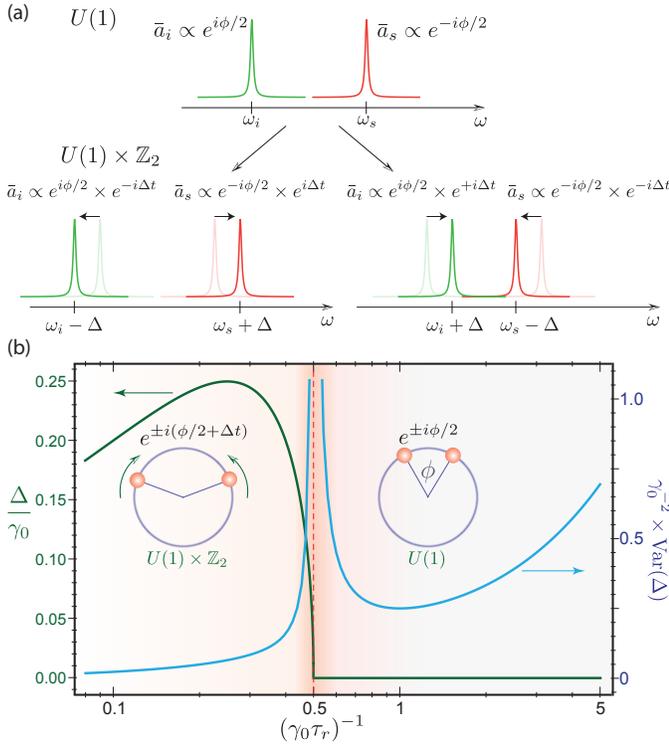
FIG. 2. (a) Schematic distinction between the $U(1)$ and the $U(1) \times \mathbb{Z}_2$ phases. The former phase is characterized by self-oscillation of the signal and idler modes with a spontaneously chosen phase difference ϕ between these modes. In contrast, the latter phase is further characterized by a limit cycle at an oscillation frequency Δ. There are two possible manifestations of such a limit cycle, corresponding to the choice of the sign of the limit cycle frequency. A particular choice of this sign spontaneously breaks the $\mathbb{Z}_2$ symmetry.
(b) The transition between the $U(1)$ and the $U(1) \times \mathbb{Z}_2$ phase versus the normalized reservoir decay rate, $(\gamma_0 \tau_r)^{-1}$. The critical point occurs at $(\gamma_0 \tau_r)^{-1} = \frac{1}{2}$, corresponding to a divergent variance, Var(Δ), of the limit cycle frequency Δ. Below this critical point, these modes no longer self-oscillate at their nominal resonances but shift to $\omega_i \to \omega_i \pm \Delta, \omega_s \to \omega_s \mp \Delta$, corresponding to a breaking of the $\mathbb{Z}_2$ symmetry (see inset, bottom). In contrast to the spontaneously chosen but constant phase difference between the two modes in the $U(1)$ phase, the phases of these modes now oscillate (see inset, top) at the frequency Δ that continuously grows from zero below the critical point. The calculations in this figure are performed for $\mu = 2$.

rate. Similarly, phase boundaries are indicated in such an analysis by a vanishing real part of the least negative eigenvalue, i.e. a divergent relaxation time. While these calculations are detailed in Appendix C, we outline the procedure and discuss the main implications of these results below.

The Heisenberg-Langevin equations can be linearized around each distinct steady state solution as $a_{i,s,P} = \bar{a}_{i,s,P} + \delta a_{i,s,P}$, where $\bar{a}_{i,s,P}$ are the respective mean field solutions in the three dynamical phases. Cast in matrix form, the response of the fluctuations $\delta a_{i,s,P}$ to the noise forces is governed by the susceptibility matrix (also referred to as the dynamical matrix [31]). As shown in [24], this analysis is more conveniently performed for the respective cross-quadratures of the signal and idler modes and takes the form $\delta \tilde{\mathbf{x}} = -(\mathbf{\Sigma}(\omega) + i\omega \mathbf{I})^{-1} \tilde{\mathbf{v}}$ (see Appendix C). The poles of the susceptibility matrix are given by complex frequencies ω satisfying $\text{Det}[\mathbf{\Sigma}(\omega) + i\omega \mathbf{I}] = 0$ and the eigenvalues of the inverse susceptibility matrix are defined as $\lambda = -i\omega$. The real part of these eigenvalues correspond to the damping rate of the system's response to generic perturbations.

This analysis, performed by linearizing the system around the disordered (PA) phase, yields the eigenvalues $\lambda_\pm = \frac{\gamma_0}{4} \left[(\mu - \frac{2}{\gamma_0 \tau_r}) \pm \sqrt{(\mu + \frac{2}{\gamma_0 \tau_r})^2 - \frac{8}{\gamma_0 \tau_r}} \right]$. Deep in the Markovian regime, $(\gamma_0 \tau_r)^{-1} \gg 1$, these eigenvalues are purely real and negative for $\mu < 1$ indicating the stability of this phase. As the reservoir coherence time is increased, the eigenvalues remain real and negative in the vicinity of the critical point $\mu = 1$ (orange curves in Fig. 3). Similar analysis can also be performed by linearizing the system around the mean field solutions for the $U(1)$ and $U(1) \times \mathbb{Z}_2$ phases indicating that these solutions too are stable to generic perturbations in their respective domains. This stability is illustrated for the three phases for representative choices of the parameter $(\gamma_0 \tau_r)^{-1}$ in Fig. 3.

In addition to confirming the stability of the mean field phases, the above analysis also sheds light on other features of this system that arise from the non-Markovian system-reservoir interactions. In particular, it reveals the emergence of new phenomenology associated with the presence of exceptional points [33, 34] in the phase diagram. For $(\gamma_0 \tau_r)^{-1} > 2$, the eigenvalues corresponding to the disordered phase are purely real and the system can be mapped onto the Markovian system. However, as the coherence time of the reservoir is increased, the eigenvalues morph into complex conjugate pairs for sufficiently small drive μ. This qualitative shift in the nature of the eigenvalues from purely real to complex conjugate values occurs at a distinct point in the system where two eigenvalues (and their corresponding eigenmodes) coalesce. Such distinct points are referred to as exceptional points and are associated with unique topological properties akin to a Berry's phase [34].

In the disordered phase, we find that the locus of excep-

4
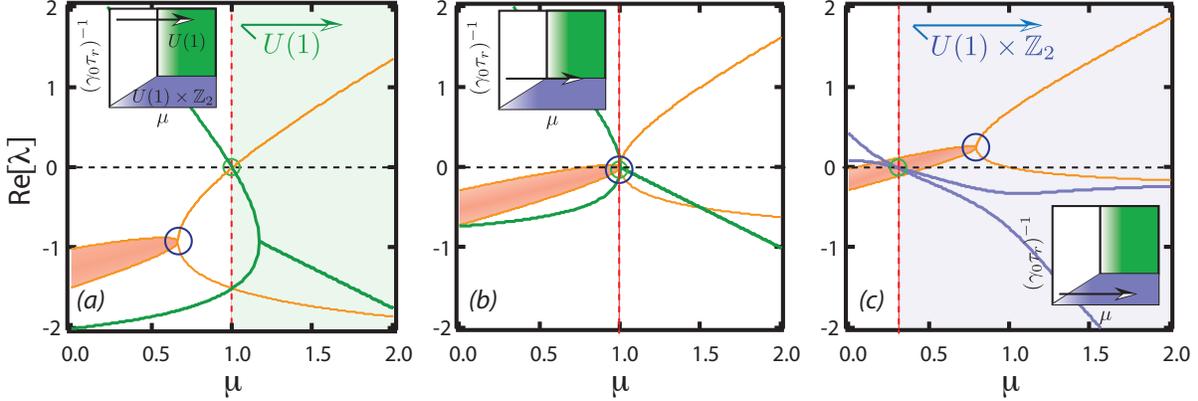
FIG. 3. The behavior of the low lying eigenspectrum corresponding to the disordered phase (orange), $U(1)$ phase (green) and $U(1) \times \mathbb{Z}_2$ phase (blue). The eigenvalues are obtained by linearizing the equations of motion around the steady state solutions in the three different phases. Shown here are two eigenvalues with the lowest negative real parts for each phase. Figures (a) to (c) demonstrate the trend with increasing reservoir coherence time τ_r showing the relative positions of the exceptional point (blue circle) and the critical point (green circle) *vs* the drive strength μ. For the disordered phase (orange traces), the imaginary part of the eigenvalue is represented as the width of the eigenmode. The exceptional point corresponds to a coalescence of the eigenvalues and eigenmodes and a vanishing imaginary part. The critical point occurs when the disordered phase becomes unstable ($\mathrm{Re}[\lambda] > 0$) and gives way to the broken symmetry phases. (a) In the regime $\frac{1}{2} < (\gamma_0 \tau_r)^{-1} < 2$, the exceptional point occurs before the critical point governing the transition to the $U(1)$ phase. The eigenvalues are purely real in the vicinity of the critical point. As such, the critical behavior in this regime can be mapped onto a supercritical pitchfork bifurcation. (b) At $(\gamma_0 \tau_r)^{-1} = \frac{1}{2}$, the exceptional point and the critical point coincide, i.e. the real and imaginary parts of the eigenvalues vanish simultaneously at the critical point, indicating the emergence of the $U(1) \times \mathbb{Z}_2$ phase. (c) Deep in the non-Markovian regime, i.e. $(\gamma_0 \tau_r)^{-1} < \frac{1}{2}$, the critical point occurs before the exceptional point and the transition to the $U(1) \times \mathbb{Z}_2$ phase occurs when the eigenvalues are purely imaginary. Here, the critical behavior corresponds to a supercritical Hopf bifurcation. The displayed eigenspectra correspond to (a) $(\gamma_0 \tau_r)^{-1} = 1.25$, (b) $(\gamma_0 \tau_r)^{-1} = 0.50$, and (c) $(\gamma_0 \tau_r)^{-1} = 0.15$.

tional points is described by the contour $(\mu \gamma_0 \tau_r + 2)^2 - 8 \gamma_0 \tau_r = 0$ (see Appendix E). Similarly, the contour of exceptional points in the $U(1)$ phase is described by the equation $4 + 4\gamma_0 \tau_r (4 - 8\mu) + ((2\mu - 3)\gamma_0 \tau_r)^2 = 0$. As seen in Fig. 1, the trajectories of these exceptional points within the disordered and $U(1)$ phase meet at the multicritical point $\mu = 1, (\gamma_0 \tau_r)^{-1} = \frac{1}{2}$. At this multicritical point, the exceptional points coincide with a critical point, i.e. both the real and imaginary parts of the eigenvalues λ simultaneously vanish, heralding the emergence of the $U(1) \times \mathbb{Z}_2$ phase.

The relative positions of the exceptional points and the phase boundary is shown in Fig. 3 for various regimes of reservoir coherence times. For small reservoir coherence time with $(\gamma_0 \tau_r)^{-1} > \frac{1}{2}$, the exceptional point occurs for pump drives $\mu < 1$. As such, the eigenvalues of the disordered phase are purely real near the critical point (Fig. 3 (a)). As the reservoir coherence time is increased, the exceptional point approaches the critical point $\mu = 1$ from below. In contrast, for large reservoir coherence times $(\gamma_0 \tau_r)^{-1} < \frac{1}{2}$, the exceptional point occurs for values of pump drive beyond the critical pump strength. As such,

the eigenvalues corresponding to the disordered phase are purely imaginary at the critical point separating the disordered phase from the $U(1) \times \mathbb{Z}_2$ phase (Fig. 3(c)). At the multicritical point $(\gamma_0 \tau_r)^{-1} = \frac{1}{2}$, the critical point $\mu_{cr} = 1$ coincides with the exceptional point and the real and imaginary parts of $\lambda_\pm$ simultaneously vanish (Fig. 3(b)), leading to non-reciprocal behavior and the simultaneous breaking of a discrete ($\mathbb{Z}_2$) symmetry in addition to the U(1) symmetry related to the signal-idler phase difference.

V. NOVEL CRITICAL BEHAVIOR

In addition to the emergence of the novel $U(1) \times \mathbb{Z}_2$ phase, the presence of the non-Markovian system-reservoir interactions also result in novel critical behavior in this system. Note that the phase diagram defines three phase transitions : the $PA - U(1)$ transition, the $PA - U(1) \times \mathbb{Z}_2$ transition, and the $U(1) - U(1) \times \mathbb{Z}_2$ transition. These phase boundaries meet at the multicritical point defined by the parameters $\mu = 1, (\gamma_0 \tau_r)^{-1} = \frac{1}{2}$.

Below, we discuss the critical behavior at each of these phase boundaries.

The $PA - U(1)$ phase transition : - In the Markovian limit of this system, i.e. $(\gamma_0 \tau_r)^{-1} \gg 1$, the transition into the $U(1)$ phase occurs at the normalized drive amplitude $\mu = 1$. Accordingly, we can define the reduced distance from criticality as $\epsilon = (\mu - 1)$. The eigenvalues λ corresponding to the disordered phase are purely real in the vicinity of the phase boundary. Moreover, the least negative eigenvalue scales near the critical point as $\lambda(\epsilon) \sim \epsilon$, thereby defining the critical exponent $\nu z = 1$ in this regime. Further, the steady-state amplitudes of the signal and idler modes in the $U(1)$ phase scale as $|a_{i,s}| \sim \sqrt{\epsilon}$, defining the critical exponent $\beta = 1/2$. Lastly, the variance of this steady-state amplitude and the susceptibility of this order parameter diverges near the phase boundary according to the relation $\mathrm{Var}(a_{i,s}) \sim |\epsilon|^{-1}$, defining the critical exponent $\gamma = 1$. These exponents are identical to the $PA - U(1)$ phase transition in the Markovian system. We also note that this phase transition can also be viewed as a supercritical pitchfork bifurcation [35].

The $PA - U(1) \times \mathbb{Z}_2$ phase transition : - In the regime $(\gamma_0 \tau_r)^{-1} < \frac{1}{2}$, the transition between the disordered phase and the $U(1) \times \mathbb{Z}_2$ phase occurs at the critical point $\mu_{cr} = \frac{2}{\gamma_0 \tau_r}$. Defining the reduced distance from criticality as $\epsilon \equiv \frac{\mu - \mu_{cr}}{\mu_{cr}}$, the eigenvalues λ corresponding to the disordered phase are purely imaginary in the vicinity of this critical point, i.e. $\lambda(\epsilon) \sim \epsilon + i(\Delta + O(\epsilon))$. Due to the nonzero limit cycle frequency Δ near the critical point, this transition corresponds to a supercritical Hopf bifurcation [36, 37] with an additional $\mathbb{Z}_2$ symmetry.

From the above discussions, it can be seen that the transition out of the disordered phase morphs from a supercritical pitchfork bifurcation for $(\gamma_0 \tau_r)^{-1} > \frac{1}{2}$ to a supercritical Hopf bifurcation for $(\gamma_0 \tau_r)^{-1} < \frac{1}{2}$. At the multicritical point $\mu = 1, (\gamma_0 \tau_r)^{-1} = 1/2$, the eigenvalues corresponding to the disordered phase coalese and the critical point coincides with an exceptional point, i.e. both the real and imaginary parts of the eigenvalues simultaneously vanish with $\lambda \sim \epsilon + 2i\sqrt{|\epsilon|}$. As such, in addition to the divergent relaxation time represented by the vanishing real part of the eigenvalue, the vanishing imaginary part sets an additional divergent timescale near criticality. This latter divergence corresponds to the period of the limit cycle in the $U(1) \times \mathbb{Z}_2$ phase at this multicritical point. Further, this divergent period of the limit cycle

at the critical point also implies that the transition cannot be mapped onto to a conventional supercritical Hopf bifurcation. The dual divergence of the relaxation and oscillation timescales, corresponding to the coincidence of a critical point with an exceptional point, is a unique feature of the non-Markovian dynamics. Additionally, the variance of the steady-state amplitudes at the multicritical point diverges as $\mathrm{Var}(a_{i,s}) \sim |\epsilon|^{-2}$, defining the critical exponent $\gamma = 2$.

The $U(1) - U(1) \times \mathbb{Z}_2$ phase transition : - The phase transition between these two phases can be accessed by tuning the normalized system-reservoir coherence time $(\gamma_0 \tau_r)^{-1}$. The phase transition occurs at $(\gamma_0 \tau_r)^{-1} = \frac{1}{2}$, and the appropriate reduced distance from criticality is given by $\epsilon_r = 2(\gamma_0 \tau_r)^{-1} - 1$. As described earlier, the limit cycle frequency Δ grows as $O(\sqrt{|\epsilon_r|})$ and the amplitude of the limit cycle is independent of the distance to the critical point. Again, these scaling relations are distinct from limit cycle behaviors found in other driven dissipative systems or a conventional supercritical Hopf bifurcation where instead, the frequency of the limit cycle scales as $O(1)$ near criticality while the amplitude of the limit cycle scales as $O(\sqrt{\epsilon})$ [35, 38, 39].

VI. ENHANCED SQUEEZING AND CORRELATIONS DUE TO NON-MARKOVIAN DYNAMICS

Next, we discuss the two-mode squeezing and entanglement in this system and the effect of non-Markovian dynamics on the observed entanglement. As is well known from prior work on this model [10, 24], the two-mode interaction results in correlations, squeezing and entanglement between quadratures of the signal and idler modes. In comparison to the corresponding Markovian system, the presence of the non-Markovian system-reservoir interactions and the appearance of the exceptional point near the $U(1) - U(1) \times \mathbb{Z}_2$ phase boundary result in an enhanced degree of entanglement between the two modes.

As shown in [24], the fluctuation spectra and two-mode correlations are obtained from the power spectral densities of the cross-quadratures via the relation $\mathbf{S}_{X,Y}(\omega) = \frac{1}{2\pi}(\tilde{\mathbf{\Sigma}}_{X,Y} + i\omega\mathbf{I})^{-1}\mathbf{D}(\tilde{\mathbf{\Sigma}}_{X,Y}^{\dagger} - i\omega\mathbf{I})^{-1}$, where the diffusion matrix is given by
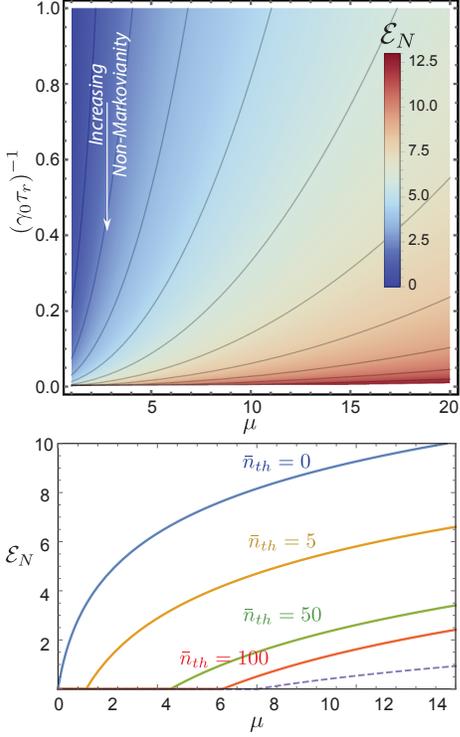
FIG. 4. (Top) The logarithmic negativity $\mathcal{E}_N$ as a measure of the bipartite entanglement [40, 41] between the signal and idler modes *vs* the drive strength μ and the normalized reservoir decay rate $(\gamma_0\tau_r)^{-1}$. (Bottom) In the $U(1)\times\mathbb{Z}_2$ phase, the entanglement between the two modes extends well beyond the quantum regime and can be observed even for large thermal occupancy of the two modes. The logarithmic negativity is shown for increasing thermal occupancy $\bar{n}_{th}$ *vs* drive strength for $(\gamma_0\tau_r)^{-1} = \frac{1}{5}$. For comparison, the logarithmic negativity for a Markovian system with $\bar{n}_{th} = 5$ is shown by the dashed line.

$$\mathbf{D} = \frac{1}{2}\begin{pmatrix} \frac{4g^2}{\gamma_0\gamma_P}\tilde{\gamma}'(\omega)(\bar{n}_{th,i}+\frac{1}{2}) & 0 & 0 \\ 0 & \frac{4g^2}{\gamma_0\gamma_P}\tilde{\gamma}'(\omega)(\bar{n}_{th,s}+\frac{1}{2}) & 0 \\ 0 & 0 & \frac{4g^2}{\gamma_0^2}\gamma_P(\bar{n}_{th,P}+\frac{1}{2}) \end{pmatrix}$$

where $\tilde{\gamma}'(\omega) = \mathrm{Re}[\tilde{\gamma}(\omega)] = \gamma_0\frac{1}{1+(\omega\tau_r)^2}$ and the thermal phonon numbers are related to the effective temperature of the modes, i.e. $\bar{n}_{th,i,s,P} = (\exp(\frac{\hbar\omega_{i,s,P}}{k_B T}) - 1)^{-1}$. The steady state variances of the cross-quadratures can be obtained from the fluctuation spectrum using the Wiener-Khintchine theorem by integrating the fluctuations,

$$\sigma_{X,Y} = \int_{-\infty}^{\infty} \mathbf{S}_{X,Y}(\omega)d\omega$$

Below threshold, the squeezed and amplified variances (normalized to the thermal variances) are respectively given by

$$\sigma_{sq} = \frac{2(\gamma_0\tau_r)^{-1}}{(1+\mu)(2(\gamma_0\tau_r)^{-1}+\mu)}$$

$$\sigma_{amp} = \frac{2(\gamma_0\tau_r)^{-1}}{(1-\mu)(2(\gamma_0\tau_r)^{-1}-\mu)}$$

The squeezed variance at steady state is minimized at

$\mu = \mu_{cr} = \min(1, 2(\gamma_0\tau_r)^{-1})$. In particular, close to the multicritical point $\mu_{cr} = 1, (\gamma_0\tau_r)^{-1} = \frac{1}{2}$, we obtain a steady state squeezing limit $\sigma_{sq} = \frac{1}{4}$, outperforming the Markovian steady-state squeezing limit of $\sigma_{sq} = \frac{1}{2}$.

Above threshold, in the $U(1)$ phase, the normalized variances of the cross-quadratures are given by

$$\sigma_{x_+} = \frac{\bar{n}_{th,P} + \frac{1}{2}}{\bar{n}_{th} + \frac{1}{2}} \frac{2(\mu-1)(\mu+(\gamma_0\tau_r)^{-1})}{\mu(2(\gamma_0\tau_r)^{-1}+2\mu-1)} + $$
$$+ \frac{(\gamma_0\tau_r)^{-1}}{\mu(2(\gamma_0\tau_r)^{-1}+2\mu-1)}$$
$$\sigma_{x_-} \to \infty$$
$$\sigma_{y_+} = \frac{\bar{n}_{th,P} + \frac{1}{2}}{\bar{n}_{th} + \frac{1}{2}} \frac{2(\mu-1+(\gamma_0\tau_r)^{-1})}{(2(\gamma_0\tau_r)^{-1}+2\mu-3)} + $$
$$+ \frac{(\gamma_0\tau_r)^{-1}}{(\mu-1)(2(\gamma_0\tau_r)^{-1}+2\mu-3)}$$
$$\sigma_{y_-} = \frac{(\gamma_0\tau_r)^{-1}}{1+2(\gamma_0\tau_r)^{-1}}$$

where $x_\pm, y_\pm$ are the cross-quadratures composed of symmetric and anti-symmetric combinations of the signal and idler quadratures (see Appendix D). Here, we have assumed that $\bar{n}_{th} \equiv \bar{n}_{th,i} \approx \bar{n}_{th,s}$.

In the $U(1) \times \mathbb{Z}_2$ phase, the non-zero limit cycle frequency Δ introduces a coupling between the nominally orthogonal cross-quadratures. Aside from this modification, the computation of the various variances proceeds as before.

By dynamically varying the pump drive strength μ on timescales short compared to γ_0^{-1} and τ_r, we can achieve a degree of transient squeezing much larger than that achievable in steady state [42]. In fact, the variance of the transiently squeezed cross-quadratures scales as $(\bar{n}_{th} + \frac{1}{2})\frac{2(\gamma_0\tau_r)^{-1}}{(1+\mu)(2(\gamma_0\tau_r)^{-1}+\mu)} \propto \frac{1}{\mu^2}$ for large drive strength, in contrast to the Markovian scaling $(\bar{n}_{th} + \frac{1}{2})\frac{1}{1+\mu} \propto \frac{1}{\mu}$, where $\bar{n}_{th}$ is the average thermal population of the signal and idler modes (see Appendix D, [24], [42]). This enhancement over a Markovian system is also reflected in the logarithmic negativity $\mathcal{E}_N = -\frac{1}{2}\log_2\left[\min(\frac{\sigma_{sq}}{\sigma_{zpm}}, 1)\right]$, where σ_{zpm} is the zero point variance of the cross-quadratures. As can be seen in Fig. 4, this enhanced degree of entanglement persists even at large thermal occupancy of the signal and idler modes. We speculate that this enhancement is due to the topological properties of the exceptional point and the non-reciprocal behavior of the system in its vicinity.

VII. CONCLUSIONS

In summary, we consider a parametrically driven two-mode quantum system and identify a class of non-Markovian system-reservoir interactions that results in the emergence of a novel broken symmetry phase in this quantum system. We analyze the phase diagram of this system and show that the emergent phase is accompanied by the appearance of exceptional points in the system. This emergent phase manifests a larger degree of two-mode entanglement than would be observed in the corresponding Markovian system. We note that the two-mode system and the form of non-Markovianity considered here are readily accessible in cavity optomechanical systems as well as various hybrid quantum systems, paving the way for experimental demonstrations of these predictions well into the quantum regime. Future work will extend this analysis to the regime of spatially multimode optomechanical systems and discuss the interplay between non-Markovian correlations, optomechanical synchronization, spatial fluctuations and driven, dissipative dynamics. In addition to realizing metrologically relevant optomechanical states, we suggest that this interplay also offers a new arena for disorder-free optomechanical realizations of dynamical phases with novel broken symmetries such as have been recently observed in spin systems [43, 44] .

Appendix A: Equations of motion

The Hamiltonian for the two-mode driven dissipative system is given by [10, 23, 24]

$$\mathcal{H}/\hbar = \sum_{k=\{i,s,P\}} \omega_k \hat{a}_k^\dagger \hat{a}_k - \chi\hat{x}_P\hat{x}_i\hat{x}_s - (F_P e^{-i\omega_P t}\hat{a}_P^\dagger + \text{h.c.})$$
(A1)

In the interaction picture with $\mathcal{H}_0/\hbar = \sum_k \omega_k \hat{a}_k^\dagger \hat{a}_k$, and making the rotating wave approximation, the interaction Hamiltonian transforms to $\mathcal{H}/\hbar = -g(\hat{a}_s^\dagger\hat{a}_i^\dagger\hat{a}_P + \hat{a}_P^\dagger\hat{a}_s\hat{a}_i) - $

$(F_P \hat{a}_P^\dagger + \text{h.c.})$ where $g = \chi x_{0,i} x_{0,s} x_{0,P}$ and $x_{0,k}$ denotes the zero-point amplitude of the respective modes. Here, we have assumed that the pump mode is actuated by a resonant, classical force and that $\omega_P = \omega_i + \omega_s$.

Further, the influence of the reservoir on these modes is incorporated through noise operators $\hat{f}$ and takes the form $\mathcal{H}_r/\hbar = -\sum_k (\hat{a}_k^\dagger \hat{f}_k + \text{h.c.})$. For the signal and idler modes, these noise forces are zero-mean, gaussian random variables whose two-point correlation is related to the dissipation kernel $\gamma(t)$ in accordance with the fluctuation dissipation theorem. Here, we assume that the signal and idler modes are in contact with a colored reservoir with a dissipation kernel given by $\gamma(t - t') = \gamma_0 \tau_r^{-1} \exp(-(t - t')/\tau_r)\Theta(t - t')$ where $\Theta(t)$ is the Heaviside step function. Accordingly, these noise forces satisfy the following relations, $\langle f_k \rangle = 0$, and $\langle f_k(t) f_l^\dagger(t') \rangle = \delta_{kl} \times (\bar{n}_{th} + 1)\frac{\gamma_0}{2\tau_r} e^{-|t-t'|/\tau_r}$ where $\bar{n}_{th} = (\exp(\frac{\hbar \omega_{i,s}}{k_B T}) - 1)^{-1}$.

In accordance with typical experimental situations in optomechanical systems [23], we assume that the pump mode is in contact with a Markovian reservoir and that its damping rate is much larger than those of the signal and idler modes, i.e. $\gamma_P \gg \gamma_0$. This leads to the Heisenberg-Langevin equations of the form

$$\dot{a}_i = -\frac{1}{2}\int_{-\infty}^t \gamma(t-t')a_i(t')dt' + iga_s^\dagger a_P + if_i \quad \text{(A2)}$$

$$\dot{a}_s = -\frac{1}{2}\int_{-\infty}^t \gamma(t-t')a_s(t')dt' + iga_i^\dagger a_P + if_s \quad \text{(A3)}$$

$$\dot{a}_P = -\frac{\gamma_P}{2}a_P + iga_i a_s + iF_P \quad \text{(A4)}$$

Here, we are ignoring the Langevin forces on the pump. As explained in [24], the pump noise can be ignored in evaluating the dynamical steady-state phases or the degree of two-mode correlations below threshold. Above threshold, this pump noise has an appreciable effect on the two-mode squeezing. In our calculations of the squeezing spectra above threshold, this pump noise is included by assuming that the pump mode is in contact with a Markovian reservoir as explained in [24].

These equations can be recast by defining the dimensionless amplitudes $A_{i,s} = a_{i,s}\frac{2g}{\sqrt{\gamma_0 \gamma_P}}$ and $A_P = a_P \frac{2g}{\gamma_0}$ to

obtain

$$\dot{A}_i = \frac{1}{2}\left[-\int_{-\infty}^t \gamma(t-t')A_i(t')dt' + i\gamma_0 A_s^* A_P + i\gamma_0 \tilde{f}_i\right] \quad \text{(A5)}$$

$$\dot{A}_s = \frac{1}{2}\left[-\int_{-\infty}^t \gamma(t-t')A_s(t')dt' + i\gamma_0 A_i^* A_P + i\gamma_0 \tilde{f}_s\right] \quad \text{(A6)}$$

$$\dot{A}_P = \frac{1}{2}\left[-\gamma_P A_P + i\gamma_P A_i A_s + i\gamma_P \mu\right] \quad \text{(A7)}$$

where $\tilde{f}_{i,s} = \gamma_0^{-1}\frac{4g}{\sqrt{\gamma_0 \gamma_P}}f_{i,s}$ and we have defined the normalized drive strength $\mu = F_P/F_{cr}$ where $F_{cr} = \frac{\gamma_P \gamma_0}{4g}$.

Appendix B: Steady state dynamical phases and mean field phase diagram

We consider the situation where the signal and idler modes are not driven, i.e. they are only subject to the Langevin forces originating from their coupling to the colored reservoir. In contrast, the pump mode is actively driven by a classical force represented by the normalized drive μ. In various regimes of the drive strength μ and the reservoir coherence time τ_r, we consider dynamical steady-state phases represented by the ansatz

$$A_{i,s} = \bar{A}_{i,s}e^{-i\Delta_{i,s}t} \quad \text{(B1)}$$
$$A_P = \bar{A}_P \quad \text{(B2)}$$

Substituting this ansatz into Eqns. (A5-A7), we obtain

$$-i\Delta_i \bar{A}_i e^{-i\Delta_i t} = -\frac{1}{2}e^{-i\Delta_i t}\bar{A}_i \tilde{\gamma}(\Delta_i) + i\frac{\gamma_0}{2}\bar{A}_s^* \bar{A}_P e^{i\Delta_s t} \quad \text{(B3)}$$

$$-i\Delta_s \bar{A}_s e^{-i\Delta_s t} = -\frac{1}{2}e^{-i\Delta_s t}\bar{A}_s \tilde{\gamma}(\Delta_s) + i\frac{\gamma_0}{2}\bar{A}_i^* \bar{A}_P e^{i\Delta_i t} \quad \text{(B4)}$$

$$0 = -\frac{1}{2}\gamma_P \bar{A}_P + i\frac{\gamma_P}{2}\bar{A}_i \bar{A}_s e^{-i(\Delta_i + \Delta_s)t} + i\frac{\gamma_P}{2}\mu \quad \text{(B5)}$$

Here, we have used the fourier transform of the dissipation kernel, $\tilde{\gamma}(\omega) = \int dt \gamma(t)e^{i\omega t} = \gamma_0(1 - i\omega\tau_r)^{-1}$.

These equations always admit the trivial solution $\bar{A}_i = \bar{A}_s = 0, \bar{A}_P = i\mu$. For dynamical steady-states with finite signal and idler amplitudes, the above equations require $\Delta_i + \Delta_s = 0$. Hence, below we define $\Delta \equiv \Delta_i = -\Delta_s$. Eqns. (B3,B4) together yield the following condition

$$\left(\frac{\tilde{\gamma}(\Delta)}{2} - i\Delta\right)\left(\frac{\tilde{\gamma}(-\Delta)}{2} + i\Delta\right)^* \bar{A}_i = \frac{\gamma_0^2}{4}|\bar{A}_P|^2 \bar{A}_i \quad \text{(B6)}$$

Since $\tilde{\gamma}(-\omega) = \tilde{\gamma}^*(\omega)$, this requires steady-state phases with non-zero signal and idler mode amplitudes to satisfy the condition

$$\left(\frac{\tilde{\gamma}(\Delta)}{2} - i\Delta\right)^2 = \frac{\gamma_0^2}{4}|\bar{A}_P|^2 \qquad (B7)$$

indicating that $\frac{\tilde{\gamma}_0}{2} \equiv \frac{\tilde{\gamma}(\Delta)}{2} - i\Delta$ is real and positive. Further, Eqns. (B3,B4) in combination with Eqn. (B5) yields the following expression for the signal and idler amplitudes,

$$\left(\frac{\tilde{\gamma}_0}{\gamma_0}\right)^2 \left[1 + 2\left|\frac{\gamma_0}{\tilde{\gamma}_0}\right||\bar{A}_{i,s}|^2 + \left|\frac{\gamma_0}{\tilde{\gamma}_0}\right|^2 |\bar{A}_{i,s}|^4\right] = \mu^2 \ (B8)$$

$$\Rightarrow |\bar{A}_{i,s}| = \sqrt{\mu - \frac{\tilde{\gamma}_0}{\gamma_0}} \qquad (B9)$$

Accordingly, we define the critical pump amplitude $\mu_{cr} = \tilde{\gamma}_0/\gamma_0$ as the drive strength beyond which the signal and idler modes develop a non-zero amplitude, i.e. the onset of parametric self-oscillation.

Lastly, given the constraint from Eqn. (B7) that $\tilde{\gamma}_0/2$ be real-valued and positive, we obtain

$$\frac{1}{2}\tilde{\gamma}(\Delta) - i\Delta = \frac{1}{2}\frac{\gamma_0}{1 + \tau_r^2\Delta^2} + i\Delta\left(\frac{1}{2}\frac{\gamma_0\tau_r}{1 + \tau_r^2\Delta^2} - 1\right) \in \mathbb{R} \tag{B10}$$

yielding $\Delta = 0$, or $\Delta = \tau_r^{-1}\sqrt{\frac{\gamma_0\tau_r}{2} - 1}$. Note that the latter solution is only meaningful for $\gamma_0 \geq 2\tau_r^{-1}$.

Based on these relations, we can identify three distinct dynamical phases in this system.

- In the regime $\gamma_0 \leq 2\tau_r^{-1}$, the coherence time of the reservoir is small compared to the intrinsic damping time of the signal/idler modes. Here, we obtain the condition $\Delta = 0$ and $\tilde{\gamma}_0 = \tilde{\gamma}(0) = \gamma_0$. Hence, the critical drive strength is given by $\mu_{cr} = 1$. In this regime, for drive strengths $\mu < 1$, the only stable phase is the trivial solution $\bar{A}_i = \bar{A}_s = 0, \bar{A}_P = i\mu$. This is the disordered or parametric amplifier phase. As the drive strength is increased beyond $\mu_{cr} = 1$, the parametric amplifier phase becomes unstable (Fig. 3(a)) and gives way to the parametric oscillator phase characterized by $\bar{A}_{i,s} = ie^{\pm i\phi/2}\sqrt{\mu - 1}, \bar{A}_P = i$. The signal-idler phase difference ϕ is unconstrained and the emergence of this parametric oscillator phase is accompanied by the spontaneous breaking of the $U(1)$

symmetry associated with the choice of this phase. As such, we denote this to be the $U(1)$ phase.

- In the regime $\gamma_0 > 2\tau_r^{-1}$, the coherence time of the reservoir is long compared to the damping time of the signal/idler modes. As seen from Eqns. (B9,B10), in this regime the critical point shifts to $\mu_{cr} = 2(\gamma_0\tau_r)^{-1} < 1$. For $\mu < \mu_{cr}$, the only stable phase is the disordered or trivial solution with $\bar{A}_{i,s} = 0$. For drive strengths $\mu_{cr} < \mu$, the disordered phase is unstable and gives way to a self-oscillating phase with non-zero Δ, given either by the solution $\bar{A}_i = ie^{i\phi/2}e^{-i\Delta t}\sqrt{\mu - \mu_{cr}}, \bar{A}_s = ie^{-i\phi/2}e^{i\Delta t}\sqrt{\mu - \mu_{cr}}, \bar{A}_P = i\mu_{cr}$ or by the solution $\bar{A}_i = ie^{i\phi/2}e^{i\Delta t}\sqrt{\mu - \mu_{cr}}, \bar{A}_s = ie^{-i\phi/2}e^{-i\Delta t}\sqrt{\mu - \mu_{cr}}, \bar{A}_P = i\mu_{cr}$, where $\Delta = \tau_r^{-1}\sqrt{\frac{\gamma_0\tau_r}{2} - 1}$. In this dynamical phase, the signal and idler modes undergo self-oscillation at frequencies that are shifted away from their nominal frequencies by an amount Δ. In addition to the breaking of the $U(1)$ symmetry associated with the choice of the signal-idler phase difference ϕ, this phase also breaks the discrete $\mathbb{Z}_2$ symmetry associated with the sign of the frequency shift Δ. As such, we denote this dynamical phase as the $U(1) \times \mathbb{Z}_2$ phase. For $\mu > 1$, all three solutions exist but the trivial solution and the $U(1)$ solution are unstable, with the $U(1) \times \mathbb{Z}_2$ solution remaining as the only stable dynamical phase.

These three dynamical phases along with the phase boundaries demarcating these phases are shown in Fig.(1) of the main text.

Appendix C: Exceptional points and stability of mean field dynamical phases

The stability of the mean-field dynamical phases to generic perturbations is demonstrated by evaluating the eigenvalues of the susceptibility matrix $\Sigma + i\omega\mathbf{I}$ as discussed in the main text. In particular, a stable dynamical phase is indicated by a susceptibility matrix whose eigenvalues have non-positive real parts. We outline the calculation of these eigenvalues for each dynamical phase below. We first distinguish between the mean amplitudes and the fluctuations by writing $A_{i,s} = (\bar{A}_{i,s} + \delta A_{i,s})e^{-i\Delta_{i,s}t}$ with the mean amplitudes in each dynamical phase given by the expressions in the previous section. The equations of motion Eqns. (A5-A7) yield

$$\partial_t \begin{pmatrix} \delta A_i \\ \delta A_s \\ \delta A_P \end{pmatrix} = \int_{-\infty}^t dt' \begin{pmatrix} -\frac{1}{2}\gamma(t-t') & 0 & i\frac{\gamma_0}{2}\bar{A}_s^*\delta(t-t') \\ 0 & -\frac{1}{2}\gamma(t-t') & i\frac{\gamma_0}{2}\bar{A}_i^*\delta(t-t') \\ i\frac{\gamma_P}{2}\bar{A}_s\delta(t-t') & i\frac{\gamma_P}{2}\bar{A}_i\delta(t-t') & -\frac{\gamma_P}{2}\delta(t-t') \end{pmatrix} \begin{pmatrix} \delta A_i(t') \\ \delta A_s(t') \\ \delta A_P(t') \end{pmatrix}$$
$$+ \begin{pmatrix} 0 & i\frac{\gamma_0}{2}\bar{A}_P & 0 \\ i\frac{\gamma_0}{2}\bar{A}_P & 0 & 0 \\ 0 & 0 & 0 \end{pmatrix} \begin{pmatrix} \delta A_i^* \\ \delta A_s^* \\ \delta A_P^* \end{pmatrix} + \frac{i}{2} \begin{pmatrix} \gamma_0 \tilde{f}_i(t) \\ \gamma_0 \tilde{f}_s(t) \\ \gamma_P \mu \end{pmatrix} \tag{C1}$$

As shown in [24], the complex fluctuations can be decomposed into real quadratures in the form $\delta \mathbf{A} = \delta\vec{\alpha} + i\delta\vec{\beta}$ such that the above equation can be recast as

$$\delta\dot{\vec{\alpha}} = \int_{-\infty}^t dt' \mathbf{M}_\alpha(t-t')\delta\vec{\alpha}(t') + \mathbf{v}_\alpha(t) \tag{C2}$$

$$\delta\dot{\vec{\beta}} = \int_{-\infty}^t dt' \mathbf{M}_\beta(t-t')\delta\vec{\beta}(t') + \mathbf{v}_\beta(t) \tag{C3}$$

where $\mathbf{v}_{\alpha,\beta}$ are the Langevin noise terms and

$$\mathbf{M}_{\alpha,\beta}(t) = \frac{1}{2} \begin{pmatrix} -\gamma(t) & \mp\gamma_0|\bar{A}_P|\delta(t) & \gamma_0|\bar{A}_s|\delta(t) \\ \mp\gamma_0|\bar{A}_P|\delta(t) & -\gamma(t) & \gamma_0|\bar{A}_i|\delta(t) \\ -\gamma_P|\bar{A}_s|\delta(t) & -\gamma_P|\bar{A}_i|\delta(t) & -\gamma_P\delta(t) \end{pmatrix} \tag{C4}$$

Further, we define cross-quadratures of the signal and idler modes according to the relations $x_\pm = (\alpha_i \pm \alpha_s)/\sqrt{2}, y_\pm = (\beta_i \pm \beta_s)/\sqrt{2}$ such that the two-mode correlations due to parametric down-conversion are manifest as amplification and squeezing of the above quadratures. The fluctuations of these cross-quadratures are related to the original quadrature fluctuations $\delta\vec{\alpha}, \delta\vec{\beta}$ via the relations

$$\delta\mathbf{X} = \mathbf{R}\delta\vec{\alpha}; \;\; \delta\mathbf{Y} = \mathbf{R}\delta\vec{\beta}; \;\; \mathbf{R} = \frac{1}{\sqrt{2}} \begin{pmatrix} 1 & 1 & 0 \\ 1 & -1 & 0 \\ 0 & 0 & \sqrt{2} \end{pmatrix} \tag{C5}$$

where $\delta\mathbf{X} = (\delta x_+, \delta x_-, \delta x_P)^T, \delta\mathbf{Y} = (\delta y_+, \delta y_-, \delta y_P)^T$. The fluctuations of the cross-quadratures are governed by the equation

$$\partial_t \delta\mathbf{X} = \int_{-\infty}^t dt' \mathbf{\Sigma}_X(t-t')\delta\mathbf{X}(t') + \mathbf{v}_X(t) \tag{C6}$$

$$\partial_t \delta\mathbf{Y} = \int_{-\infty}^t dt' \mathbf{\Sigma}_Y(t-t')\delta\mathbf{Y}(t') + \mathbf{v}_Y(t) \tag{C7}$$

where $\mathbf{\Sigma}_{X,Y} = \mathbf{R}\mathbf{M}_{\alpha,\beta}\mathbf{R}^T$ and $\mathbf{v}_{X,Y} = \mathbf{R}\mathbf{v}_{\alpha,\beta}$. By moving to the frequency domain, the above equations can be recast as

$$\begin{pmatrix} \delta\tilde{x}_+ \\ \delta\tilde{x}_- \\ \delta\tilde{x}_P \\ \delta\tilde{y}_+ \\ \delta\tilde{y}_- \\ \delta\tilde{y}_P \end{pmatrix} = -(\mathbf{\Sigma} + i\omega\mathbf{I})^{-1}\tilde{\mathbf{v}} \tag{C8}$$

where $\delta\tilde{x}_+$ denotes the fourier transform of δx_+ etc. and

$$\mathbf{\Sigma}(\omega) = \begin{pmatrix} \tilde{\mathbf{\Sigma}}_X & 0 \\ 0 & \tilde{\mathbf{\Sigma}}_Y \end{pmatrix} \tag{C9}$$

We note that in the $U(1) \times \mathbb{Z}_2$ phase where $\Delta \neq 0$, the susceptibility matrix does not remain block diagonal due to correlations between the various cross-quadratures. However, the procedure for evaluating the eigenvalues and stability remains the same.

The poles of the susceptibility matrix are defined by complex ω satisfying $\text{Det}[-\mathbf{\Sigma} - i\omega\mathbf{I}] = 0$ and the eigenvalues of the inverse susceptibility matrix are defined as $\lambda = -i\omega$. The real part of these eigenvalues corresponds to the damping rate of the system's response to generic perturbations. As such, the stability of the mean field dynamical phases is indicated by a non-positive real part of the eigenvalues. Critical points governing continuous transitions between distinct dynamical phases is indicated by a vanishing of this real part or equivalently, a divergent relaxation time. The linearization around the trivial (parametric amplifier) solution yields the eigenvalues

$$\lambda_\pm = \frac{\gamma_0}{4}\left[(\mu - \frac{2}{\gamma_0\tau_r}) \pm \sqrt{(\mu + \frac{2}{\gamma_0\tau_r})^2 - \frac{8}{\gamma_0\tau_r}}\right] \tag{C10}$$

As such, for $(\gamma_0\tau_r)^{-1} > 2$, the eigenvalues are purely real and the system can be mapped onto the Markovian system. As the coherence time of the reservoir is increased, the eigenvalues morph into complex conjugate pairs for sufficiently small drive strength μ. This change from real eigenvalues to complex conjugate eigenvalues occurs at a point where the two eigenvalues (and corresponding

eigenmodes) coalesce. Such points are called exceptional points. In this system, the exceptional point approaches the critical point from below as the coherence time τ_r is increased. For $(\gamma_0\tau_r)^{-1} = \frac{1}{2}$, the exceptional point and the critical point coincide at $\mu = 1$. This heralds the emergence of the $U(1) \times \mathbb{Z}_2$ phase. For even larger reservoir coherence times, $(\gamma_0\tau_r)^{-1} < \frac{1}{2}$, the exceptional point occurs beyond the critical point governing the transition from the disordered phase to the $U(1) \times \mathbb{Z}_2$ phase. This behavior of the exceptional point relative to the critical point is depicted in Fig. 3 of the main text.

Similar linearization can also be performed around the $U(1)$ and the $U(1) \times \mathbb{Z}_2$ phases using the formalism described above. The calculations, while straightforward, are laborious and are not reproduced here. The real parts of the respective eigenvalues as a function of drive strength μ and normalized reservoir coherence time $(\gamma_0\tau_r)^{-1}$ are shown in Fig. 3. As can be seen, the real parts of the eigenvalues of the susceptibility matrix for these phases are negative for large μ indicating that these dynamical phases are indeed stable to generic perturbations.

The Markovian case is retrieved from Eqn.(C10) in the limit $\tau_r \to 0$, i.e. $\lambda_+ = \frac{\gamma_0}{2}(\mu - 1)$. Note that $\lambda_- \to 1/\tau_r$ corresponds to the rate at which the reservoir follows the system, and can be adiabatically eliminated in the limit of small τ_r. The exponent with which λ vanishes, $\lambda \sim |\epsilon|$, where $\epsilon = (\mu - \mu_{cr})/\mu_{cr}$ is the reduced distance from criticality, defines the conventional critical exponent νz for the phase transition: $\nu z = 1$ in the Markovian case. In contrast, for $(\gamma_0\tau_r)^{-1} = 1/2$, the eigenvalues are

$$\lambda_\pm = \frac{\gamma_0}{4}\left[(\mu - 1) \pm \sqrt{(\mu - 1)(\mu + 3)}\right] \qquad (C11)$$

and thus scale near criticality as

$$\lambda_\pm = \frac{\gamma_0}{4}\left[\epsilon \pm \sqrt{\epsilon(4 + \epsilon)}\right] \approx \frac{\gamma_0}{4}\left[\epsilon \pm 2i\sqrt{-\epsilon}\right] \sim \epsilon \pm 2i\sqrt{|\epsilon|} \qquad (C12)$$

Both the real and imaginary part of the eigenvalue vanish at criticality, with the real part being proportional to $|\epsilon|$ and the imaginary part being proportional to $\sqrt{|\epsilon|}$. While the divergent dissipation timescale is set by the vanishing real part, and also occurs in the Markovian case, the vanishing imaginary part of λ sets an additional divergent *oscillation* timescale for the system near criticality. This novel critical behavior is solely attributable to the non-Markovianity of the system-bath interactions.

For $(\gamma_0\tau_r)^{-1} < 1/2$, i.e. across the $PA - U(1) \times \mathbb{Z}_2$ phase transition, the eigenvalues are

$$\lambda_\pm = \frac{\gamma_0}{4}\left[(\mu - \mu_{cr}) \pm i(\Delta + O(\mu - \mu_{cr}))\right] \qquad (C13)$$

where $\mu_{cr} = \frac{2}{\gamma_0\tau_r} < 1$ and $\Delta = 2\sqrt{\mu_{cr}(1 - \mu_{cr})} = \tau_r^{-1}\sqrt{\frac{\gamma_0\tau_r}{2} - 1}$. In particular, while the real part does vanish at criticality ($\mu \to \mu_{cr}$), its imaginary part remains finite at $\Delta > 0$. As such, $\lambda(\epsilon) \sim \epsilon + i\Delta \sim \epsilon + iO(1)$ as $\epsilon \to 0$. Due to the finite limit cycle frequency at the critical point, this phase boundary can be associated with a supercritical Hopf bifurcation [35].

Appendix D: Two-mode correlations and entanglement in the steady state and transient regime

As shown in [24], the fluctuation spectra and two-mode correlations are obtained from the power spectral densities of the cross-quadratures via the relation

$$\mathbf{S}_{X,Y}(\omega) = \frac{1}{2\pi}(\tilde{\mathbf{\Sigma}}_{X,Y} + i\omega\mathbf{I})^{-1}\mathbf{D}(\tilde{\mathbf{\Sigma}}_{X,Y}^\dagger - i\omega\mathbf{I})^{-1} \quad (D1)$$

where the diffusion matrix is given by

$$\mathbf{D} = \frac{1}{2}\begin{pmatrix} \frac{4g^2}{\gamma_0\gamma_P}\tilde{\gamma}'(\omega)(\bar{n}_{th,i} + \frac{1}{2}) & 0 & 0 \\ 0 & \frac{4g^2}{\gamma_0\gamma_P}\tilde{\gamma}'(\omega)(\bar{n}_{th,s} + \frac{1}{2}) & 0 \\ 0 & 0 & \frac{4g^2}{\gamma_0^2}\gamma_P(\bar{n}_{th,P} + \frac{1}{2}) \end{pmatrix}$$

where $\tilde{\gamma}'(\omega) = \text{Re}[\tilde{\gamma}(\omega)] = \gamma_0\frac{1}{1+(\omega\tau_r)^2}$ and the thermal phonon numbers are related to the effective temperature of the modes, i.e. $\bar{n}_{th,i,s,P} = (\exp(\frac{\hbar\omega_{i,s,P}}{k_B T}) - 1)^{-1}$. The

steady state variances of the cross-quadratures can be obtained from the fluctuation spectrum using the Wiener-

Khintchine theorem by integrating the fluctuations,

$$\sigma_{X,Y} = \int_{-\infty}^{\infty} \mathbf{S}_{X,Y}(\omega)d\omega \qquad (D2)$$

Below threshold, the squeezed and amplified variances (normalized to the thermal variances) are respectively given by

$$\sigma_{sq} = \frac{2(\gamma_0\tau_r)^{-1}}{(1+\mu)(2(\gamma_0\tau_r)^{-1}+\mu)} \qquad (D3)$$

$$\sigma_{amp} = \frac{2(\gamma_0\tau_r)^{-1}}{(1-\mu)(2(\gamma_0\tau_r)^{-1}-\mu)} \qquad (D4)$$

For a given $(\gamma_0\tau_r)^{-1}$, the squeezed variance below threshold is minimized at $\mu = \mu_{cr} = \min(1, 2(\gamma_0\tau_r)^{-1})$. In particular, close to the multicritical point $\mu_{cr} = 1, (\gamma_0\tau_r)^{-1} = \frac{1}{2}$, we obtain a steady state squeezing limit $\sigma_{sq} = \frac{1}{4}$, outperforming the Markovian steady-state squeezing limit of $\sigma_{sq} = \frac{1}{2}$.

To achieve a squeezing better than this steady-state minimum, we can implement a transient protocol, where the pump drive strength μ is set to a value larger than

μ_{cr} for a period of time that is short compared to γ_0^{-1}. Within this short duration, pump depletion and saturation effects can be neglected. The amplified quadrature grows with an exponential envelope, and the squeezed quadrature decays with an exponential envelope to the asymptote given by the expression above, yielding a dependence of $\sigma_{sq} \propto \frac{1}{\mu^2}$ for large drive amplitudes. This protocol works when the absolute amplitude of motion is small enough that the linearization around the disordered solution remains valid.

Note that by setting $\tau_r \to 0$, we recover the Markovian case expressions. In particular, the degree of squeezing is $\sigma_{sq} = \frac{1}{1+\mu}$, and the divergence of the amplified quadrature is $\sigma_{amp} = \frac{1}{1-\mu} = \frac{1}{|\mu-\mu_{cr}|} \sim \frac{1}{|\epsilon|}$. In other words, the divergence of the amplified fluctuations has an exponent -1 in $|\epsilon|$ in the Markovian limit. In contrast, for $(\gamma_0\tau_r)^{-1} = 1/2$, the divergence of σ_{amp} has an exponent -2, i.e. $\sigma_{amp} = \frac{1}{(1-\mu)^2} \sim \frac{1}{|\epsilon|^2}$. A change in this exponent compared to the Markovian case is another signature of novel critical behavior induced by the non-Markovian system-bath interactions.

Above threshold, in the $U(1)$ phase, the normalized variances of the various cross-quadratures are given by

$$\sigma_{x_+} = \frac{\bar{n}_{th,P} + \frac{1}{2}}{\bar{n}_{th} + \frac{1}{2}} \frac{2(\mu-1)(\mu+(\gamma_0\tau_r)^{-1})}{\mu(2(\gamma_0\tau_r)^{-1}+2\mu-1)} + \frac{(\gamma_0\tau_r)^{-1}}{\mu(2(\gamma_0\tau_r)^{-1}+2\mu-1)} \qquad (D5)$$

$$\sigma_{x_-} \to \infty \qquad (D6)$$

$$\sigma_{y_+} = \frac{\bar{n}_{th,P} + \frac{1}{2}}{\bar{n}_{th} + \frac{1}{2}} \frac{2(\mu-1+(\gamma_0\tau_r)^{-1})}{(2(\gamma_0\tau_r)^{-1}+2\mu-3)} + \frac{(\gamma_0\tau_r)^{-1}}{(\mu-1)(2(\gamma_0\tau_r)^{-1}+2\mu-3)} \qquad (D7)$$

$$\sigma_{y_-} = \frac{(\gamma_0\tau_r)^{-1}}{1+2(\gamma_0\tau_r)^{-1}} \qquad (D8)$$

where we have assumed that $\bar{n}_{th} \equiv \bar{n}_{th,i} \approx \bar{n}_{th,s}$.

In the $U(1) \times \mathbb{Z}_2$ phase, the non-zero frequency shifts Δ introduce correlations between the nominally uncorrelated Langevin forces in orthogonal cross-quadratures. In addition, as mentioned previously, this frequency shift also introduces time-dependent correlations between the various cross-quadratures. Aside from these modifications, the computation of the various variances proceeds as before. The final expressions are cumbersome and not reproduced here.

Lastly, the logarithmic negativity is obtained from the squeezed variances as $\mathcal{E}_N = -\frac{1}{2}\log_2\left[\min(\frac{\sigma_{sq}}{\sigma_{zpm}}, 1)\right]$, where σ_{zpm} is the zero point variance of the cross-

quadratures. These results are shown in Fig. 4 of the main text.

Appendix E: Trajectory of exceptional points in the phase diagram

In general, the non-Markovian equations of motion are more challenging to solve analytically than the Markovian equations. The exponential non-Markovian kernel $\gamma(t-t')$ considered in this work, however, allows for the definition of auxiliary variables which greatly simplifies calculations. Defining $h_{i,s} = \int_{-\infty}^{t} \frac{1}{\tau_r}e^{-(t-t')/\tau_r}a_{i,s}(t')dt'$

and its dimensionless version $H_{i,s} = h_{i,s}\frac{2g}{\sqrt{\gamma_0\gamma_P}}$, the semi-classical equations of motion in Eqns. (A5-A7) are simplified to a set of first order differential equations –

$$\dot{A}_i = \frac{1}{2}\left[-\gamma_0 H_i + i\gamma_0 A_s^* A_P + i\gamma_0 \tilde{f}_i\right] \quad \text{(E1)}$$

$$\dot{H}_i = -H_i/\tau_r + A_i/\tau_r \quad \text{(E2)}$$

$$\dot{A}_s = \frac{1}{2}\left[-\gamma_0 H_s + i\gamma_0 A_i^* A_P + i\gamma_0 \tilde{f}_s\right] \quad \text{(E3)}$$

$$\dot{H}_s = -H_s/\tau_r + A_s/\tau_r \quad \text{(E4)}$$

$$\dot{A}_P = \frac{1}{2}\left[-\gamma_P A_P + i\gamma_P A_i A_s + i\gamma_P \mu\right] \quad \text{(E5)}$$

These equations can be further simplified in the mean-field, i.e. in the limit of zero noise, $\tilde{f}_{i,s} \to 0$.

In the disordered PA phase below threshold ($\mu \leq \max[1, 2/\gamma_0\tau_r]$), A_P can be adiabatically eliminated as $A_P \approx i\mu$, as derived earlier. The complex Eqns. (E1-E4) can then be block diagonalized into decoupled blocks formed by the pair of cross-quadratures ($B := A_i - A_s^*, H_B := H_i - H_s^*$) and ($C := A_i + A_s^*, H_C := H_i + H_s^*$). Within the parameter space of B, H_B, the equations of motion are simply

$$\begin{pmatrix} \dot{B} \\ \dot{H}_B \end{pmatrix} = \begin{pmatrix} \gamma_0\mu/2 & -\gamma_0/2 \\ 1/\tau_r & -1/\tau_r \end{pmatrix} \begin{pmatrix} B \\ H_B \end{pmatrix} \quad \text{(E6)}$$

The exceptional points of this dynamical matrix can easily be evaluated by explicitly solving for the eigenvalues and eigenvectors. We find that they coalesce along the contour defined by $(\tau_r\gamma_0\mu + 2)^2 - 8\tau_r\gamma_0 = 0$. Only one of the roots of this quadratic equation $((\gamma_0\tau_r)^{-1} = 1 - \mu/2 + \sqrt{1-\mu})$ is inside disordered phase. It corresponds to the eigenmode of the system and reservoir with the least negative real part of the eigenvalue, and is shown by the dotted contour for $\mu < 1$ in Fig.(1) of the main text. The eigenvalues along this contour of exceptional points is $\sqrt{\gamma_0/(2\tau_r)} - 1/\tau_r$ with the eigenvector $(\sqrt{\gamma_0\tau_r/2}, 1)^T$.

We can similarly compute the exceptional points in the $U(1)$ phase ($\mu \geq 1, (\gamma_0\tau_r)^{-1} \geq 1/2$). We linearize the equations of motion about the steady state solution evaluated earlier, i.e. $\bar{A}_{i,s} = ie^{\pm i\phi/2}\sqrt{\mu-1}, \bar{A}_P = i$. Writing $H_{i,s}$ in terms of real quadratures, i.e. $H_{i,s} = H_{x,i,s} + iH_{y,i,s}$, and denoting the deviations from steady state values with prefix δ, the real quadratures $\delta y_+ = (\delta y_i + \delta y_s)/\sqrt{2}$ (see also Eqn. (C5)) and $\delta H_{y_+} = (\delta H_{y,i} + \delta H_{y,s})/\sqrt{2}$ evolve according to

$$\begin{pmatrix} \dot{\delta y_+} \\ \dot{H}_{y_+} \end{pmatrix} = \begin{pmatrix} -\gamma_0(2\mu-3)/2 & -\gamma_0/2 \\ 1/\tau_r & -1/\tau_r \end{pmatrix} \begin{pmatrix} \delta y_+ \\ H_{y_+} \end{pmatrix} \quad \text{(E7)}$$

The contour of exceptional points in the $U(1)$ phase is thus defined by $4 + \tau_r\gamma_0(4 - 8\mu) + ((2\mu - 3)\gamma_0\tau_r)^2 = 0$. Both roots of this quadratic equation yield valid solutions in the $U(1)$ phase. One of them $((\gamma_0\tau_r)^{-1} = \mu - 1/2 + \sqrt{2(\mu - 1)})$, which corresponds to the system and reservoir's eigenmode with the least negative real part of the eigenvalue, is shown by the dotted contour for $\mu > 1$ in Fig.(1) of the main text. The eigenvalues and eigenvectors are, again, $\sqrt{\gamma_0/(2\tau_r)} - 1/\tau_r$ and $(\sqrt{\gamma_0\tau_r/2}, 1)^T$, respectively.

Appendix F: Critical behavior of the limit cycle frequency Δ

As described earlier, the limit cycle phase emerges in the regime $(\gamma_0\tau_r)^{-1} < 1/2$. Below this phase boundary, the limit cycle frequency is given by $\Delta = \tau_r^{-1}\sqrt{\frac{\gamma_0\tau_r}{2} - 1}$. Parametrizing the distance from the phase boundary as $\epsilon_r \equiv 2(\gamma_0\tau_r)^{-1} - 1$, we see that the order parameter Δ scales as $\Delta \sim |\epsilon_r|^{1/2}$ with the critical exponent $\beta = 1/2$.

For noise small compared to the steady state amplitude R, we can approximate the phase fluctuations as $\delta\phi_{i,s} = \delta\alpha_{i,s}/R$ (see Eqn. (C5), [24]). We can thus express the the phase difference as $\phi = \phi_i - \phi_s = \delta\phi_i - \delta\phi_s = \sqrt{2}\delta x_-/R$, where $x_- := (\alpha_s - \alpha_i)/\sqrt{2}$. Its spectrum is $S_{\phi,\phi} = \frac{2}{R^2}S_{x_-,x_-}(\omega)$, with $S_{x_-,x_-}(\omega) = \frac{1}{2\pi}(\tilde{\Sigma}_{x_-,x_-} + i\omega\mathbf{I})^{-1}\mathbf{D}(\tilde{\Sigma}_{x_-,x_-}^\dagger - i\omega\mathbf{I})^{-1}$. The limit cycle frequency $\Delta = \frac{1}{2}(\dot{\phi}_i - \dot{\phi}_s)$ thus has a spectrum $S_{\Delta,\Delta} = \frac{\omega^2}{4}S_{\phi,\phi}(\omega) = \frac{\omega^2}{2R^2}S_{x_-,x_-}(\omega)$.

In the $U(1)$ phase, the power spectral density of the cross quadrature δx_- with unit thermal noise is given by

$$S_{x_-,x_-}(\omega) = \frac{1}{2\pi}\frac{4\gamma_0}{\omega^2(4 - 4\tau_r\gamma_0 + \tau_r^2(\gamma_0^2 + 4\omega^2))} \quad \text{(F1)}$$

A factor of $1/\omega^2$ here signifies that the phase difference $\phi \propto x_-$ undergoes diffusion. Note also that this quadrature does not have a μ dependence. Thus, the variance of the order parameter and hence, the susceptibility of the order parameter in the vicinity of the phase boundary is given by

$$\text{Var}(\Delta) = \frac{1}{2R^2}\int_{-\infty}^{\infty} d\omega \frac{1}{2\pi}\frac{4\gamma_0}{(4 - 4\tau_r\gamma_0 + \tau_r^2(\gamma_0^2 + 4\omega^2))}$$

$$= \frac{1}{2R^2}\frac{1}{2\tau_r^2(1/(\gamma_0\tau_r) - 1/2)} \quad \text{(F2)}$$

$$\Rightarrow \text{Var}(\Delta) \sim [(\gamma_0\tau_r)^{-1} - 1/2]^{-1} \sim |\epsilon_r|^{-1} \quad \text{(F3)}$$

This yields the critical exponent $\gamma = 1$.

This divergent variance of the limit cycle frequency is depicted in Fig.(2) of the main text.

Appendix G: RG flow under time rescaling

It is instinctive to think that the finite system-bath interaction timescale τ_r would rescale to zero under a RG flow, thereby taking the system to the Markovian limit of $\tau_r \to 0$. In this section, we show that the system has a RG fixed point (source) in the phase space of $(\mu, (\gamma_0\tau_r)^{-1})$ at the multicritical point $(1, 1/2)$ (see Fig. (1) of the main text). This fixed point is clearly distinct from the Markovian fixed point at $(\gamma_0\tau_r)^{-1} \to \infty$, and as shown below, the flow around this point can push the system further away from the Markovian limit.

The first order differential equations of motion in the disordered PA phase in the zero noise limit, derived earlier as Eqn.(E6), can be recast as a second order differential equation in B as

$$\ddot{B}(t) = (\frac{\gamma_0\mu}{2} - \frac{1}{\tau_r})\dot{B}(t) + \frac{\gamma_0}{2\tau_r}(\mu - 1)B(t) \qquad \text{(G1)}$$

Rescaling time by b, as $t' = t/b$, we get

$$\frac{1}{b^2}\ddot{B}(t') = \frac{1}{b}(\frac{\gamma_0\mu}{2} - \frac{1}{\tau_r})\dot{B}(t') + \frac{\gamma_0}{2\tau_r}(\mu - 1)B(t') \quad \text{(G2)}$$

Note that being a linear equation, B is itself not rescaled. In order to maintain the functional form of Eqn.(G1), the renormalized parameters $(\gamma_0', \tau_r', \mu')$ should satisfy

$$\frac{\gamma_0'\mu'}{2} - \frac{1}{\tau_r'} = b(\frac{\gamma_0\mu}{2} - \frac{1}{\tau_r}) \qquad \text{(G3)}$$

$$\frac{\gamma_0'}{2\tau_r'}(\mu' - 1) = b^2\frac{\gamma_0}{2\tau_r}(\mu - 1) \qquad \text{(G4)}$$

Note that these two equations are under-determined in $(\gamma_0', \tau_r', \mu')$. However, in order to focus on how the system-bath interaction timescale τ_r rescales under this time-rescaling, and how the system flows in the $(\mu, (\gamma_0\tau_r)^{-1})$ parameter space, we fix the parameter γ_0, i.e. constrain

$\gamma_0' = \gamma_0$. Note that γ_0 signifies the total strength of dissipation, i.e. $\int_0^\infty dt\gamma(t) = \gamma_0$.

We solve Eqns.(G3-G4) for (μ', τ_r') and evaluate the flow as the vector field $(\frac{d}{db}\mu', \frac{d}{db}(\gamma_0\tau_r')^{-1})$. This flow is shown in Fig.(5). The open red circle marks the unstable fixed point at $(\mu = 1, (\gamma_0\tau_r)^{-1} = 1/2)$, the multicritical point of Fig.(1) of the main text. The flow around this fixed point indicates that the ratio $(\gamma_0\tau_r)^{-1}$ can flow to either larger or smaller values, i.e. the system can
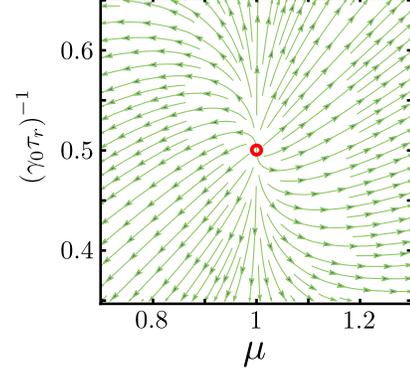
FIG. 5. RG flow of the system following a rescaling of time, shown in the $(\mu, (\gamma_0\tau_r)^{-1})$ parameter space. The open red circle marks an unstable fixed point at the multicritical point $(\mu = 1, (\gamma_0\tau_r)^{-1} = 1/2)$, distinct from the Markovian fixed point that occurs at $(\gamma_0\tau_r)^{-1} \to \infty$. Contrary to intuition, the flow shows that under time rescaling, the finite system-bath interaction timescale need not rescale to zero (the Markovian limit).

rescale either toward or farther from the Markovian limit of $(\gamma_0\tau_r)^{-1} \to \infty$.

Note that the above analyses is done by linearizing the system around the disordered PA solution. While this analysis correctly predicts the presence of the multicritical point at $\mu = 1, (\gamma_0\tau_r)^{-1} = 1/2$ and the emergence of the limit cycle phase for $(\gamma_0\tau_r)^{-1} < 1/2$, the interpretation of the RG flow deep within the $U(1)$ phase or the $U(1)\times\mathbb{Z}_2$ phase would require the linearization of the RG equations about the respective steady solutions in those phases, and is not considered here.

[1] Á. Rivas and S. F. Huelga. Open quantum systems : An introduction. *arXiv:1104.5242*, 2011.
[2] I. de Vega and D. Alonso. Dynamics of non-Markovian open quantum systems. *Rev. Mod. Phys.*, 89:15001, 2017.
[3] P. Schindler, M. Müller, D. Nigg, J. T. Barreiro, E. A. Martinez, M. Hennrich, T. Monz, S. Diehl, P. Zoller, and R. Blatt. Quantum simulation of open-system dynamical maps with trapped ions. *Nature Phys.*, 9:361, 2012.
[4] Z. Xiang, S. Ashhab, J. Q. You, and F. Nori. Hybrid quantum circuits : Superconducting circuits interacting with other quantum systems. *Rev. Mod. Phys.*, 85:623, 2013.

[5] M. Aspelmeyer, T. J. Kippenberg, and F. Marquardt. Cavity optomechanics. *Rev. Mod. Phys.*, 86:1391, 2014.

[6] G. Kurizki, P. Bertet, Y. Kubo, K. Mølmer, D. Petrosyan, P. Rabl, and J. Schmiedmayer. Quantum technologies with hybrid systems. *PNAS*, 112:3866, 2015.

[7] S. Diehl, A. Micheli, A. Kantian, B. Kraus, H. P. Büchler, and P. Zoller. Quantum states and phases in driven open quantum systems with cold atoms. *Nature Phys.*, 4:878, 2008.

[8] M. Müller, S. Diehl, G. Pupillo, and P. Zoller. Engineered open systems and quantum simulations with atoms and ions. *Adv. At. Mol. Opt. Phys.*, 61:1, 2012.

[9] A. Tomadin, S. Diehl, M. D. Lukin, P. Rabl, and P. Zoller. Reservoir engineering and dynamical phase transitions in optomechanical arrays. *Phys. Rev. A*, 86:033821, 2012.

[10] P. D. Drummond and K. Dechoum. Universality of quantum critical dynamics in a planar optical parametric oscillator. *Phys. Rev. Lett.*, 95:083601, 2005.

[11] M. Wouters and I. Carusotto. Goldstone mode of optical parametric oscillators in planar semiconductor microcavities in the strong-coupling regime. *Phys. Rev. A*, 76:043807, 2007.

[12] C. Emary and T. Brandes. Chaos and the quantum phase transition in the Dicke model. *Phys. Rev. E*, 67:066203, 2003.

[13] K. Baumann, C. Guerlin, F. Brennecke, and T. Esslinger. Dicke quantum phase transition with a superfluid gas in an optical cavity. *Nature*, 464:1301, 2010.

[14] J. Klinder, H. Kessler, M. Wolke, L. Mathey, and A. Hemmerich. Dynamical phase transition in the open Dicke model. *PNAS*, 112:3290, 2015.

[15] R. H. Dicke. Coherence in spontaneous radiation processes. *Phys. Rev.*, 93:99, 1954.

[16] H. J. Lipkin, N. Meshkov, and A. J. Glick. Validity of many-body approximation methods for a solvable model : (i). exact solutions and perturbation theory. *Nucl. Phys.*, 62:188, 1965.

[17] K. Dechoum, P. D. Drummond, S. Chaturvedi, and M. D. Reid. Critical fluctuations and entanglement in the nondegenerate parametric oscillator. *Phys. Rev. A*, 70:053807, 2004.

[18] E. G. Dalla Torre, E. Demler, T. Giamarchi, and E. Altman. Quantum critical states and phase transitions in the presence of non-equilibrium noise. *Nature Phys.*, 6:806, 2010.

[19] D. Nagy, G. Szirmai, and P. Domokos. Critical exponent of a quantum-noise-driven phase transition : The open-system Dicke model. *Phys. Rev. A*, 84:043637, 2011.

[20] D. Nagy and P. Domokos. Critical exponent of quantum phase transitions driven by colored noise. *Phys. Rev. A*, 94:063862, 2016.

[21] D. M. Reich, N. Katz, and C. P. Koch. Exploiting non-markovianity for quantum control. *Sci. Rep.*, 5:12430, 2015.

[22] M. Cianciaruso, S. Maniscalco, and G. Adesso. Role of non-markovianity and backflow of information in the speed of quantum evolution. *Phys. Rev. A*, 96:012105, 2017.

[23] Y. S. Patil, S. Chakram, L. Chang, and M. Vengalattore. Thermomechanical two-mode squeezing in an ultrahigh Q membrane resonator. *Phys. Rev. Lett.*, 115:017202, 2015.

[24] S. Chakram, Y. S. Patil, and M. Vengalattore. Multimode phononic correlations in a nondegenerate parametric amplifier. *New Journal of Phys.*, 17:063018, 2015.

[25] U. Weiss. *Quantum dissipative systems*. World Scientific, 2008.

[26] J. Léonard, A. Morales, P. Zupancic, T. Esslinger, and T. Donner. Supersolid formation in a quantum gas breaking a continuous translational symmetry. *Nature*, 543:87, 2017.

[27] I. Wilson-Rae. Intrinsic dissipation in nanomechanical resonators due to phonon tunneling. *Phys. Rev. B*, 77:245418, 2008.

[28] S. Groeblacher, A. Trubarov, N. Prigge, G. D. Cole, M. Aspelmeyer, and J. Eisert. Observation of non-Markovian micro-mechanical Brownian motion. *Nature Comm.*, 6:7606, 2015.

[29] F. Bariani, S. Singh, L. F. Buchmann, M. Vengalattore, and P. Meystre. Hybrid optomechanical cooling by atomic lambda systems. *Phys. Rev. A*, 90:033838, 2014.

[30] F. Bariani, H. Soek, S. Singh, M. Vengalattore, and P. Meystre. Atom-based coherent quantum-noise cancellation in optomechanics. *Phys. Rev. A*, 92:043817, 2015.

[31] E. M. Kessler, G. Giedke, A. Imamoglu, S. F. Yelin, M. D. Lukin, and J. I. Cirac. Dissipative phase transition in a central spin system. *Phys. Rev. A*, 86:012116, 2012.

[32] M. Höning, M. Moos, and M. Fleischhauer. Critical exponents of steady-state phase transitions in fermionic lattice models. *Phys. Rev. A*, 86:013606, 2012.

[33] T. Kato. *Perturbation theory for linear operators*. Springer Berlin, 1966.

[34] W. D. Heiss. The physics of exceptional points. *J. Phys. A: Math. Theor.*, 45:444016, 2012.

[35] S. Strogatz. *Nonlinear dynamics and chaos*. Perseus, 1994.

[36] J. E. Marsden and M. McCracken. *The Hopf Bifurcation and its applications*. Springer-Verlag, 1976.

[37] J. Guckenheimer and P. Holmes. *Nonlinear Oscillations, Dynamical Systems, and Bifurcations of Vector Fields*. Springer-Verlag, 1983.

[38] M. J. Bhaseen, J. Mayoh, B. D. Simons, and J. Keeling. Dynamics of nonequilibrium Dicke models. *Phys. Rev. A*, 85:013817, 2012.

[39] C. Chan, T. E. Lee, and S. Gopalakrishnan. Limit-cycle phase in driven-dissipative spin systems. *Phys. Rev. A*, 91:051601(R), 2015.

[40] A. Peres. Separability criterion for density matrices. *Phys. Rev. Lett.*, 77:1413, 1996.

[41] M. B. Plenio. Logarithmic Negativity : A full entanglement monotone that is not convex. *Phys. Rev. Lett.*,

95:090503, 2005.

[42] H. F. H. Cheung, Y. S. Patil, L. Chang, S. Chakram, and M. Vengalattore. Nonlinear phonon interferometry at the Heisenberg limit. *arXiv:1601.02324*, 2016.

[43] S. Choi, J. Choi, R. Landig, G. Kucsko, H. Zhou, J. Isoya, F. Jelezko, S. Onoda, H. Sumiya, V. Khemani, C. von Keyserlingk, N. Y. Yao, E. Demler, and M. D. Lukin. Observation of discrete time-crystalline order in a disordered dipolar many-body system. *Nature*, 543:221, 2017.

[44] J. Zhang, P. W. Hess, A. Kyprianides, P. Becker, A. Lee, J. Smith, G. Pagano, I.-D. Potirniche, A. C. Potter, A. Vishwanath, N. Y. Yao, and C. Monroe. Observation of a discrete time crystal. *Nature*, 543:217, 2017.